

## Excitability of a Semiconductor Laser by a Two-Mode Homoclinic Bifurcation

H. J. Wünsche,<sup>1</sup> O. Brox,<sup>2</sup> M. Radziunas,<sup>1,3</sup> and F. Henneberger<sup>1</sup>

<sup>1</sup>*Humboldt-Universität zu Berlin, Institut für Physik, Invalidenstrasse 110, D-10115 Berlin, Germany*

<sup>2</sup>*Heinrich-Hertz-Institut für Nachrichtentechnik Berlin, Einsteinufer 37, D-10587 Berlin, Germany*

<sup>3</sup>*Weierstraß-Institut für Angewandte Analysis und Stochastik Berlin, Mohrenstrasse 39, D-10117, Berlin, Germany*

(Received 14 May 2001; published )

We report on the preparation of optical excitability in a distributed feedback semiconductor laser. The device integrates a single-mode laser and a 250  $\mu\text{m}$  long passive section with cleaved facet. The phase of the light fed back from the passive section is tunable by current. The theoretical analysis shows an ultimate hop between external cavity modes within every phase cycle that is associated with a two-mode homoclinic bifurcation close to which the system becomes excitable. This excitability is clearly demonstrated in the experimental response to optical injection comparing well with simulation calculations.

DOI:

PACS numbers: 42.55.Px, 42.65.Pc, 42.65.Sf

Excitability of nonlinear dynamical systems is currently a subject of intense investigations. Spiking of neurons, spreading excitations in the cardiac muscle tissue, or the Belousov-Zhabotinsky reaction are examples from biology and chemistry. Recently, driven both by fundamental and practical goals, excitability of optical systems has attracted much interest. Theoretical predictions for various configurations (bistable cavity [1], laser with saturable absorber [2] or external feedback [3]) are opposed by much less experimental work. The observation of excitability of a laser diode with external feedback is still under debate [4–9]. Here, the length of the external cavity comprises typically  $10^5$  optical wavelengths. This gives rise to an intricate and puzzling many time-scale scenario [10], where the solitary laser mode couples to a quasicontinuum of external cavity modes resulting in power dropouts and low-frequency oscillations.

The present work is based on a semiconductor laser with short external cavity. The device consists of two sections of comparable length (cf. Fig. 2). A single mode laser with distributed feedback (DFB) is supplemented by a passive phase section [11] with a cleaved facet as end mirror. The bandgap of the active section is at lower photon energies, thus avoiding pumping of the passive region by the laser emission. Carrier injection in the passive part enables one to tune the optical phase fed back in the active region. First, contrary to a laser with distant external feedback, this design allows excellent mode control. Second and equally important, in this way the topology of the phase space can be experimentally defined for preparing a desired nonlinear dynamical behavior. Stable self-pulsations in single-mode as well as two-mode regimes have been previously demonstrated both experimentally and theoretically with similar multisection devices [11–13].

The standard treatment of lasers with delayed feedback is due to the Lang-Kobayashi equations [14]. However, in the present case, the feedback is not weak, nor is the time delay much longer than the inverse mode spacing. Instead, a spatiotemporal structure develops across the en-

tire device, which has to be properly accounted for. An adequate description is given by the traveling wave equations (TWE)

$$\left(-\frac{i}{v_g} \frac{\partial}{\partial t} \mp i \frac{\partial}{\partial z} + \beta - i \frac{\alpha_0}{2}\right) \Psi_{\pm} + \kappa \Psi_{\mp} = p_{\pm} \quad (1)$$

for the slowly varying amplitudes  $\Psi_{+}(t, z)$  and  $\Psi_{-}(t, z)$  of the forward and back traveling waves, respectively ( $v_g$ : photon group velocity,  $\kappa$ : real coupling coefficient of the index grating, and  $\alpha_0$ : wave guide losses).  $\beta(t, z)$  is the instantaneous local propagation constant of the waveguide relative to the reference value  $\beta_0 = \pi/\Lambda$  determined by the period  $\Lambda$  of the Bragg grating.  $p_{\pm}(z, t)$  are amplitudes of dispersive polarization contributions not contained in  $\beta$  [15]. In the passive section,  $p_{\pm}$  is zero and  $\beta$  is an external parameter  $\beta_p = 2\pi n_{\text{eff}} c/\lambda - \beta_0$ , controlled experimentally by the phase current ( $I_p$  in Fig. 2) adjusting the effective refractive index  $n_{\text{eff}}$  appropriately [11]. In the laser section, the polarization equations

$$\frac{\partial}{\partial t} p_{\pm} = i\omega_g p_{\pm} - \frac{p_{\pm}}{\tau_p} - i\Gamma\gamma\Psi_{\pm} \quad (2)$$

yield a Lorentzian contribution to the optical gain of half-width  $1/\tau_p$  and height  $2\gamma\tau_p$  centered at  $\omega_g$ . Furthermore, in the laser section the nondispersive background propagation constant

$$\beta = \frac{1}{2}(\alpha_H + i) \frac{\Gamma g' [N - N_{tr}]}{1 + \varepsilon \Gamma \langle \Psi, \Psi \rangle} - i\Gamma\gamma\tau_p \quad (3)$$

is dynamically coupled to the average carrier density  $N(t)$ , in turn linked to the optical fields via rate equation

$$\frac{\partial N}{\partial t} = \frac{I}{eV} - \frac{N}{\tau} - 2v_g \text{Im}[\langle \Psi, \beta \Psi \rangle - \langle \Psi, p \rangle]. \quad (4)$$

( $\alpha_H$ : Henry factor,  $\Gamma$ : transverse confinement factor,  $g'$ : differential gain,  $N_{tr}$ : transparency density,  $\varepsilon$ : gain saturation coefficient,  $I$ : injection current,  $V$ : volume of the active zone,  $\tau$ : carrier lifetime, and  $\langle \Psi, \Phi \rangle$ : average of  $\Psi_{+}^* \Phi_{+} + \Psi_{-}^* \Phi_{-}$  over the laser section.)

Using compound cavity modes changing adiabatically with carrier density [12], Eqs. (1)–(4) can be transformed into a set of ordinary differential equations, enabling application of path finding algorithms and bifurcation analysis. The bifurcation parameter is the optical phase shift  $\varphi = 2\beta_p L_p$  with  $L_p$  as the phase section length.

Figure 1 displays the stationary solution for  $N$  as a function of  $\varphi$  using device parameters appropriate to the laser structure studied experimentally below. Three branches coexist in a certain range of  $\varphi$ . At  $\varphi = A$ , the two lower branches 1 and 1' are born in a saddle-node bifurcation. This bifurcation is generic for the present system and associated with an ultimate mode hop when  $\varphi$  is tuned from 0 to  $2\pi$ . Close to  $A$ , branches 1 and 1' belong to the same mode; i.e., when increasing  $N$  from 1 to 1', the optical field changes continuously. Branch 2 belongs to a different mode. The complex amplitudes of both modes together with the carrier density span the relevant five dimensional phase space.

Between points  $A$  and  $B$ , both branches 1 and 2 are stable, giving rise to hysteresis. In addition to the stationary states, a saddle-type limit cycle and a stable limit cycle (not displayed in Fig. 1) exist in some range of

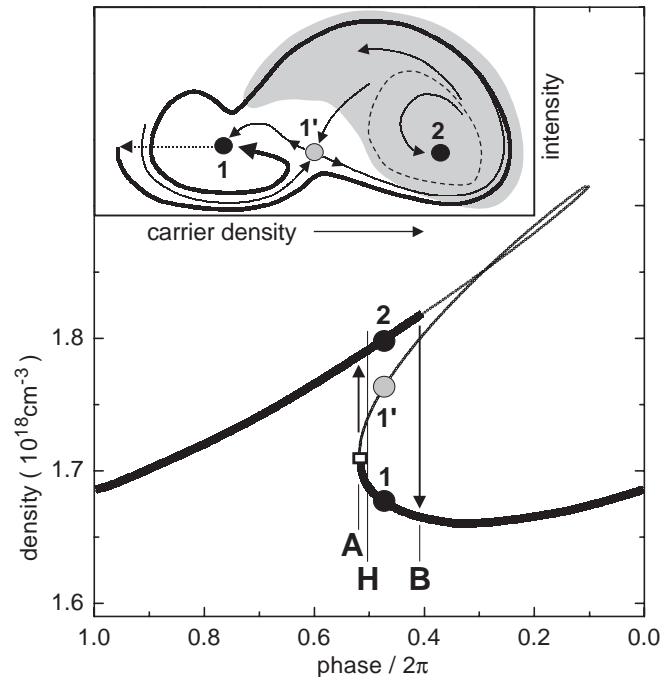


FIG. 1. Plot of carrier density of stationary states versus phase shift as calculated from Eqs. (1)–(4). Thick line: stable; thin line: unstable. Parameters:  $v_g = c/3.8$ ,  $\alpha_0 = 25 \text{ cm}^{-1}$  (laser) and  $20 \text{ cm}^{-1}$  (phase),  $\kappa = 180 \text{ cm}^{-1}$ ,  $\Gamma = 0.3$ ,  $g' = 5 \times 10^{-16} \text{ cm}^2$ ,  $I = 50 \text{ mA}$ ,  $V = 9.9 \times 10^{-11} \text{ cm}^{-3}$ ,  $\alpha_H = -5$ ,  $\varepsilon = 0$ ,  $N_{tr} = 1.3 \times 10^{18} \text{ cm}^{-3}$ ,  $\tau = 1 \text{ ns}$ , 30% facet reflectivity of phase section,  $\tau_p = 125 \text{ fs}$ ,  $\gamma = 2.6 \times 10^{15} \text{ cm}^{-1} \text{ s}^{-1}$ , and  $\omega_g$  at the long wave border of the stop band of the DFB section. Inset: phase space portrait; explanations are given in the text.

phases around  $A$ . The two cycles annihilate in a fold bifurcation left of  $A$ . In a point  $H$  just right of  $A$ , the stable orbit disappears in a homoclinic bifurcation involving saddle 1'. The Fig. 1 inset sketches a projection of the phase space topology beyond  $H$  onto the density-intensity plane. Mode 2 dominates the optical field in the grey area, otherwise mode 1. Focus 2 is surrounded by the saddle-type periodic orbit (dashed line). One root of the unstable manifold of saddle 1' leads directly to focus 1. The other root undertakes a large excursion through the domain of mode 2 before returning back to focus 1. Excitability occurs just in this situation with the stable manifold of the saddle 1' serving as separatrix. A sufficient decrease of  $N$  by external perturbation (dotted arrow) brings the system to a phase loop (thick solid line) starting beyond the separatrix, passing below the saddle, and following the big excursion of its stable manifold on the way to focus 1.

The experimental setup is schematically depicted in Fig. 2. The laser section of the device is  $220 \mu\text{m}$  long and emits at  $1536 \text{ nm}$ . The  $250\text{-}\mu\text{m}$ -long phase section has a bandgap of  $1300 \text{ nm}$ . A mode-locked fiber ring laser was used to generate pulses at a center wavelength of  $1542 \text{ nm}$  serving as external perturbation. The pulse duration is  $35 \text{ ps}$  and the repetition rate  $15 \text{ MHz}$ . An optical attenuator was used to precisely control pulse power at the device input. The pulses were launched via a circulator into the active section. The time response was analyzed at port 3 of the circulator using a fast photodiode and monitored by a sampling oscilloscope of  $50 \text{ GHz}$  bandwidth. The electrical injection on both device sections was thoroughly adjusted in order to prepare the system close to the critical region of the phase-density diagram of Fig. 1.

Figure 3 summarizes screen shots for two levels of optical injection. Below a critical pulse fluence of  $P_0 \approx 3 \text{ pJ}$ , smooth and rapidly damped relaxation oscillations of about  $6 \text{ GHz}$  are merely present. A slight increase in the optical input causes striking changes in the dynamic

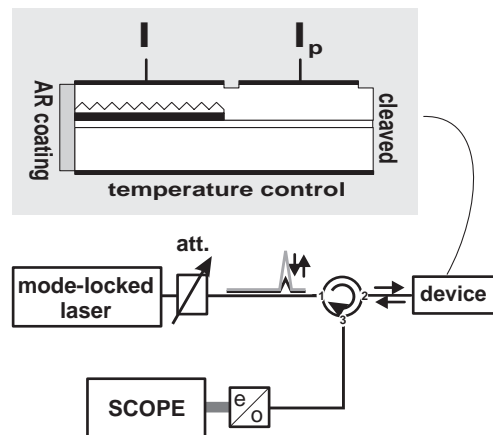


FIG. 2. Schematics of the experiment. Upper panel: device. Lower panel: optical setup. Explanations are given in the text.

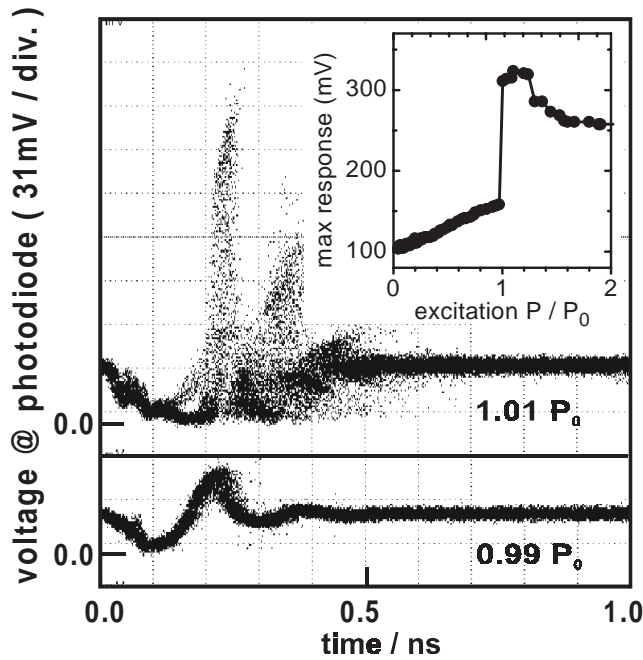


FIG. 3. Dynamic device response directly taken from the oscilloscope screen for two levels of optical injection. Inset: magnitude of the response peak vs strength of the optical excitation pulse.

response. The device emits distinct spikes being 1 order of magnitude above average output and representing direct evidence for excitability. The distinct excitability threshold is more clearly seen in the Fig. 3 inset. The two-mode nature is confirmed by the optical spectrum, where a second mode with 0.7-nm separation appears indeed above threshold. Slightly moving the phase current away from the excitability point, the device switches to a self-pulsation mode, verifying the presence of a stable limit cycle. In the absence of optical injection, when tuning the phase shift over a wider range via the phase injection current, the cw output exhibits hysteresis, consistent with the overall theoretical model.

A numerical solution of the TWE confirms the above observations. Rectangular shaped optical pulses of 30-ps duration were mimicked by using an appropriate boundary condition at the facet. As shown in Fig. 4, the experimental response is very well reproduced. The beating during pulse injection is due to a 5-nm redshift of the input photons relative to laser mode 1. The phase space view of the solution shown in the inset also corresponds well to the qualitative picture given in Fig. 1. The separation between modes 1 and 2 found in the numerical simulations is 0.6 nm and hence also in good accord with the experiment. Between the 30-ps injection and the subsequent spike emission, the device does not respond on any extra perturbation, signifying a refractory time of about 0.3 ns, markedly smaller than the carrier lifetime. Spontaneous emission noise does not noticeably affect the above results as has been checked by numerical control simulations.

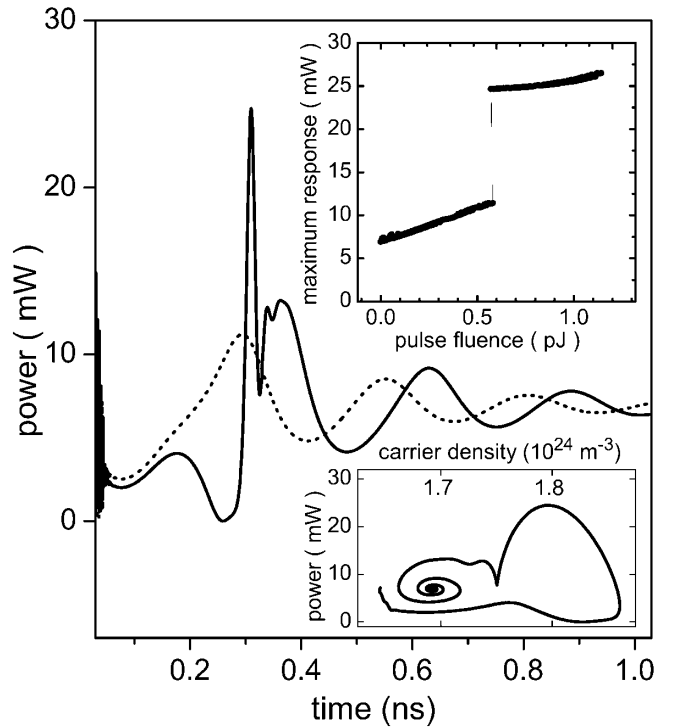


FIG. 4. Dynamic response calculated for a situation corresponding to Fig. 3. Dotted line:  $P = 0.54$  pJ; solid line:  $P = 0.63$  pJ. Lower inset: phase space view of the solution after the end of the exciting impulse. Upper inset: spike intensity versus fluence  $P$  of optical input pulses. Parameter as in Fig. 1 except  $\varepsilon = 10^{-23}$  m<sup>3</sup>.

As in the measurement, the spikes show a distinct jitter although nominally identical impulses were injected. This is related to a slowdown of the transit time close to the saddle of about 100 ps. Seemingly, this transit time depends sensitively on small fluctuations in the input regime, e.g., due to different optical phases of the input waves relative to the lasing oscillation. The calculations yield a duration of about 15 ps for the individual spikes. Resolution of their shape is therefore beyond the 50-GHz bandwidth of our detection system, whereas the longer jitter is clearly seen. The replica following the main spike in the experiment may be caused by the dip in the phase space trajectory giving rise to the two-peak shape in the calculated response. Other possibilities are a second passage of the limit cycle or multipulse excitability [16]. Clarification of the details is beyond the scope of this Letter and will be given elsewhere.

Summarizing, we have prepared excitability of a semiconductor laser. Its occurrence is related to a mode hop in a two-section device, integrating laser, and external mirror on a 100- $\mu$ m-length scale. Our experimental and theoretical analysis has demonstrated distinct features characteristic for excitable systems: (i) reaction to a perturbation by large response, (ii) existence of a threshold above which the large response appears, (iii) weak dependence of the response on the magnitude of the

perturbation above threshold, and (iv) existence of a refractory time during which the device ignores any input. It will be interesting to study multisection laser structures with respect to other novel nonlinear dynamical scenarios.

This work was partly supported by the Deutsche Forschungsgemeinschaft. We thank Bernd Sartorius for his continuous support and Martin Möhrle for providing the device. Furthermore, we acknowledge valuable discussions with Klaus Schneider and his co-workers.

- 
- [1] Weiping Lu *et al.*, Phys. Rev. A **58**, R809 (1998).
  - [2] J. L. A. Dubbeldam *et al.*, Phys. Rev. E **60**, 6580 (1999).
  - [3] M. C. Eguia and G. B. Mindlin, Phys. Rev. E **60**, 1551 (1999).
  - [4] M. Giudici *et al.*, Phys. Rev. E **55**, 6414 (1997).

- [5] G. H. M. van Tartwijk and I. Fischer, Phys. Rev. E **58**, 4041 (1998).
- [6] M. Giudici *et al.*, Phys. Rev. E **58**, 4043 (1998).
- [7] G. Giacomelli *et al.*, Phys. Rev. Lett. **84**, 3298 (2000).
- [8] J. Hales *et al.*, Phys. Rev. Lett. **85**, 78 (2000).
- [9] E. A. Viktorov and P. Mandel, Phys. Rev. Lett. **85**, 3157 (2000).
- [10] D. W. Sukow *et al.*, Phys. Rev. A **60**, 667 (1999).
- [11] B. Sartorius *et al.*, IEEE Photonics Technol. Lett. **7**, 1261 (1995).
- [12] H. Wenzel *et al.*, IEEE J. Quantum Electron. **32**, 69 (1996).
- [13] M. Radziunas *et al.*, IEEE J. Quantum Electron. **36**, 1026 (2000); M. Möhrle *et al.* (to be published).
- [14] R. Lang and K. Kobayashi, IEEE J. Quantum Electron. **16**, 347 (1980).
- [15] U. Bandelow *et al.*, IEEE J. Quantum Electron. **37**, 183 (2001).
- [16] S. Wieczorek, B. Krauskopf, and D. Lenstra, report (appeared on-line as <http://www.enm.bris.ac.uk/anm/preprints/2001r14.html> after submission of this Letter).